Research on the Optimization Design of Spiral Groove Hydrodynamic Radial Bearings Based on Aerodynamic Analysis

Zhiqiang Dong, Yiheng Chen, Yifei Dong

Abstract—In the optimization design of spiral groove radial dynamic pressure air bearings, establishing a connection between bearing capacity and bearing parameters through aerodynamic analysis is the most straightforward and effective approach. The optimization algorithm directly utilizes aerodynamic calculations in each iteration; however, automatic meshing often struggles to meet the demands of complex operating conditions, resulting in high overall computational costs. This paper employs a finite set of aerodynamic analysis results to train an artificial neural network. By integrating the particle swarm optimization algorithm into the neural network training, we introduce an improved particle swarm neural network (IPSO) to establish an approximate relationship between bearing capacity and the parameters of the gas dynamic pressure air bearing. When combined with genetic algorithm optimization, this method identifies the optimal combination of bearing parameters for maximum bearing capacity. Aerodynamic analysis reveals that the bearing capacity with the optimized parameters shows a 3.9% improvement compared to the original parameters at a speed of 100,000 RPM, with increases of 10.3% and 3.6% in bearing capacity at low and high speeds, respectively. The results indicate that this optimization design method is highly relevant and beneficial for the design of dynamic pressure air bearings.

Index Terms—Spiral groove radial bearing, CFD, Fluent, Load capacity, Optimization algorithm

I. INTRODUCTIO

Spiral groove dynamic pressure radial air bearing is a kind of high performance bearing that operates based on the principle of gas dynamic pressure lubrication. The spiral groove structure on the inner surface of the bearing sleeve directs gas is guided to form a stable gas film when the journal rotates at high speeds, enabling non-contact support. Its working principle depends on the pumping effect and gas compression of the spiral groove, which results in an uneven pressure distribution that provides radial bearing capacity.

Manuscript received June 14, 2025; revised September 11, 2025.

This work was supported in part by the Shanxi Province Fundamental Research Program of China under Grant 2022203021221152.

Zhiqiang Dong is a professor at the School of Transportation and Vehicle Engineering, Taiyuan University of Science and Technology. Address: Taiyuan 030024, China (corresponding author to provide phone: 86-18335149923; e-mail: 1786545820@qq.com).

Yiheng Chen is a postgraduate student at the School of Transportation and Vehicle Engineering, Taiyuan University of Science and Technology, Taiyuan 030024, China (e-mail: s202324211132@stu.tyust.edu.cn).

Yifei Dong is a postgraduate student at the School of Transportation and Vehicle Engineering, Taiyuan University of Science and Technology, Taiyuan 030024, China (e-mail: 1424237680@qq.com).

The parameters of the bearing are critical factors influencing its load-bearing capacity, and the design and optimization of these parameters are essential for enhancing the performance of the spiral groove hydrodynamic journal bearing.

II. RELATED WORKS

A significant amount of research has been conducted on the design of dynamic pressure radial bearing both domestically and internationally. Dong Yinghuai [1] investigated the airflow characteristics of gas bearings under various geometric parameters and operating conditions through numerical simulations. He compared the gap pressure distribution and load capacity of the bearings. Zhang Le [2] employed computational fluid dynamics (CFD) to evaluate the performance of radial sliding bearings with different spiral groove configurations, analyzing the changes in bearing capacity at various offset angles. Shi Jiahao [3] proposed an optimization design scheme for surface texture based on a particle swarm optimization algorithm, aimed at reducing the friction coefficient of the journal component and enhancing the bearing capacity of the thrust component. Ultimately, the overall lubrication performance and service life of the bearing are improved through the optimization of surface texture design. Wang Bin [4] studied the dynamic characteristics of smooth surface, herringbone groove, and foil hydrodynamic gas bearings through fluid-solid coupling simulations, parameter optimization, and experimental verification. This research provides a theoretical basis and optimization direction for enhancing the performance of gas bearings. The key parameters of a spiral hydrodynamic groove bearing primarily include the spiral angle, gas film clearance, groove width, and groove depth. Additionally, the presence of eccentricity significantly affects the bearing's load capacity. Currently, most studies examining the impact of bearing structural parameters on performance employ a single-factor experimental approach. This method has limitations when calculating bearing capacity under the influence of multiple factors. Optimal values for a variable can only be determined when that variable changes while all other variables remain constant. In the design of spiral groove bearing parameters, the existence of the pumping effect and the rarefied gas effect highlights the substantial limitations of the single-factor experimental method in addressing bearing capacity. Therefore, it is essential to consider multi-parameter optimization.

In order to determine the geometric parameters for maximum bearing capacity, this paper trains an artificial neural network that incorporates an optimized particle swarm optimization algorithm. It proposes an optimization strategy that combines the improved particle swarm optimization algorithm (IPSO) with the BP [5] neural network to address the nonlinear challenges associated with the optimization design of dynamic pressure radial bearing parameters in spiral grooves. Utilizing Plackett-Burman experimental design and an optimal Latin hypercube design with five variables, the study identifies the geometric parameters that significantly influence the bearing capacity of spiral groove hydrodynamic radial bearings. The IPSO-BP model is trained using Fluent [6] simulation data from ANSYS to establish the relationship between independent variables and optimization objectives. Additionally, genetic algorithms (GA) are employed for multi-objective optimization to determine the geometric parameters that yield the maximum bearing capacity for the spiral groove [7] hydrodynamic journal bearing. The findings provide valuable insights for enhancing the bearing capacity of spiral groove bearings.

III. METHOD

A. Structural Principles

Spiral grooves are commonly used hydrodynamic features in mechanical engineering. They typically consist of multiple helical grooves arranged either around the circumference or along the axis of a rotating surface. When relative motion occurs, these grooves pump fluid from low-pressure areas to high-pressure areas, creating a fluid film with a pressure gradient. This self-pumping action generates a hydrodynamic supporting force that significantly enhances the load-bearing capacity and stability of the friction pair. The design parameters of the spiral grooves directly affect their fluid transport capability and the resulting pressure distribution. By optimizing these parameters, benefits such as reduced friction coefficients, higher critical speeds, and improved resistance to disturbances can be achieved.

Fig 1 illustrates the spiral groove hydrodynamic bearing. As the journal and sleeve rotate relative to one another, gas is compressed, generating pressure that enhances the bearing's load capacity. The bearing has a length of L, a diameter of D, and an average gas film thickness of h When the spindle operates, it creates an eccentricity distance e and an eccentricity e between the spindle and the journal. This eccentricity results in a wedge-shaped gap between the shaft and the journal, allowing gas to flow into the narrow space during extrusion, which leads to the formation of a high-pressure zone and a low-pressure zone.

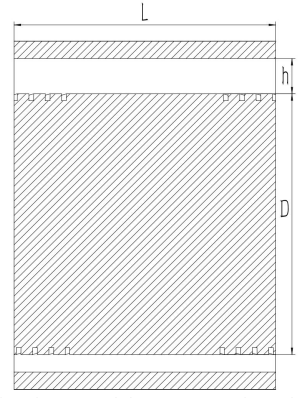


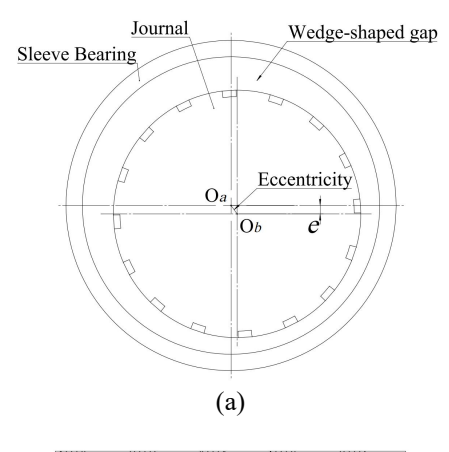
Fig 1. Schematic Diagram of the Cross-section of a Radial Bearing.

The formula for calculating eccentricity is shown in equation (1):

$$\varepsilon = \frac{e}{c} \tag{1}$$

In the equation (1), e is the eccentric distance, defined as the direct distance from the center of the journal to the center of the bearing. Meanwhile, c denotes the radial clearance, which is the difference [8] in radius between the inner diameter of the bearing and the outer diameter of the journal.

Fig 2 illustrates the expansion diagram of the working face of a spiral groove hydrodynamic bearing. Fig (a) Radial cross-sectional diagram of the air bearing, Fig (b) axial perspective view of the air bearing. O_a represents the center of the journal, while O_b denotes the center of the shaft. The widths of the spiral groove and the table are indicated as b_g and b_r , respectively. The angle formed between the spiral groove and the bearing section is referred to as the spiral angle β .



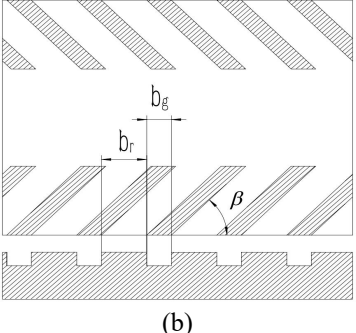


Fig 2. Unfolded View of the Working Surface of the Spiral Groove Dynamic Pressure Radial Bearing.

B. Determination of Initial Parameters and Extraction of Fluid Regions

Table I illustrates the chosen parameters for bearing design:

TABLE I
INITIAL SPECIFICATIONS OF SPIRAL GROOVE DYNAMIC PRESSURE BEARINGS

Geometric parameters	Value
bearing diameter D/mm	30
bearing length L/mm	30
air film gap h/μm	15
flute length L/mm	11
flute width W/mm	2.5
flute depth $M/\mu m$	13
flute number	16
eccentricity	0.3
spiral angle β / $^{\circ}$	45

Fig 3 illustrates the flow field area. A 3D model of the spiral groove dynamic pressure radial bearing has been created in SolidWorks, featuring a rotor and an outer wall structure with 16 slots. The spiral groove dynamic pressure gas bearing is then extracted using Space Claim in ANSYS software to identify the smooth region of the gas film [9], which represents the air bearing.

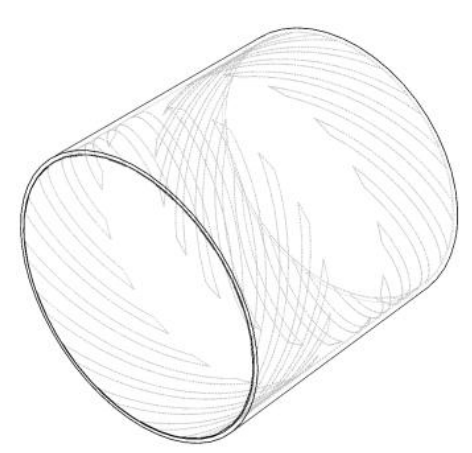


Fig 3. Air Membrane Flow Field Area.

C. Calculation of Equations

The pressure distribution of the air layer can be determined by solving the Navier-Stokes equations. The Navier-Stokes equations are presented in equation (2):

$$\begin{cases} \rho \frac{du}{dt} = \rho X - \frac{\partial p}{\partial x} + \eta \nabla^2 u + \eta \frac{1}{3} \frac{\partial}{\partial x} (divu) \\ \rho \frac{dv}{dt} = \rho Y - \frac{\partial p}{\partial x} + \eta \nabla^2 v + \eta \frac{1}{3} \frac{\partial}{\partial y} (divu) \\ \rho \frac{dw}{dt} = \rho Z - \frac{\partial p}{\partial x} + \eta \nabla^2 w + \eta \frac{1}{3} \frac{\partial}{\partial z} (divu) \end{cases}$$
(2)

Included in this are the air density, with u, v, and w representing the velocity components in the x, y, and z directions, respectively. X, Y, and Z denote the unit volume forces in the x, y, and z directions, respectively. Additionally, p refers to the gas film pressure, and η signifies the dynamic viscosity of the gas.

$$\nabla^2 = \frac{\partial^2}{\partial x^2} + \frac{\partial^2}{\partial y^2} + \frac{\partial^2}{\partial z^2}$$
 is a Pilates operator.

 $\operatorname{div} u = \frac{\partial u}{\partial x} + \frac{\partial v}{\partial y} + \frac{\partial w}{\partial z}$ is the divergence of velocity.

The equation for bearing capacity is expressed in formula (3):

$$W = \iint p dA \tag{3}$$

In the equation (3), dA denotes a small surface area element of the gas film.

IV. EXPERIMEN

A. Grid Division

In the meshing process, a hexahedral mesh is utilized to partition the gas film flow field of the spiral groove hydrodynamic journal bearing. A high-quality mesh significantly enhances the stability of numerical simulations [10]. Hexahedral grids provide several advantages over other grid types, including a consistent structure, uniform unit shape, and organized node distribution. These features enable a more accurate representation of minor flow field variations during the simulation of complex flow scenarios [11], while

also minimizing numerical dissipation and error accumulation. Fig 4 illustrates the meshing of the spiral groove hydrodynamic radial bearing. Fig (a) illustrates the complete mesh segmentation of the air-floating bearing, while Fig (b) provides a detailed view of the local mesh segmentation of the air-floating bearing.

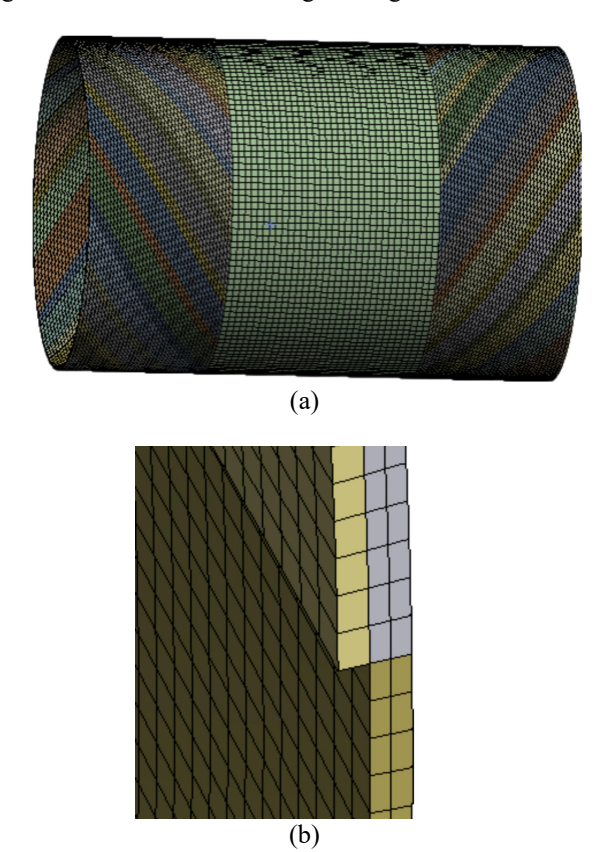


Fig 4. Overall and Local Mesh Division of the Spiral Groove Dynamic Pressure Radial Bearing.

B. Grid Independence Verification

As the number of grids increases, the accuracy of the simulation demonstrates a phased change pattern. Initially, accuracy improves with the addition of more grids, but eventually stabilizes [12]. Once the grid density reaches a specific threshold, further increases in density have minimal impact on the simulation results, indicating that the results are effectively independent of the grid at this density. In this experiment, a total of 833,330 grids were utilized, and the verification of grid independence is illustrated in Fig 5.

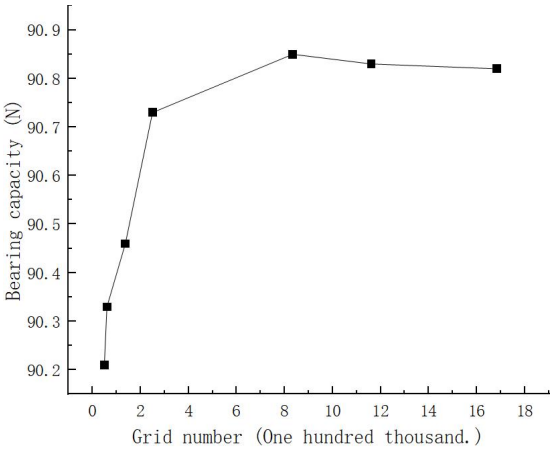


Fig 5. Comparison of Grid Independence Verification.

C. Numerical Solutions

A pressure-based solver is employed [13]. The inlet and outlet are configured as pressure inlet and pressure outlet, both set to a pressure of 101,325 Pa. The outer wall of the bearing is designated as static [14], while the inner wall is configured to rotate at a speed of 100,000 RPM. The SIMPLE algorithm is utilized, and the iterative accuracy is set to the default value.

D. Calculation Results and Analysis

(1) The Effect of Different Helical Angles on the Bearing Gas Film Load Capacity

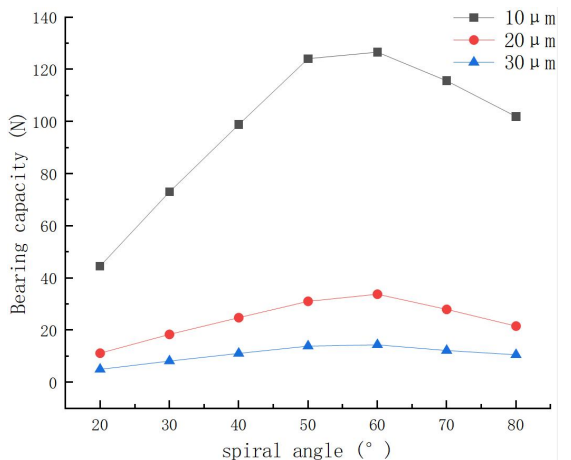


Fig 6. The Relationship Between Different Air Film Thicknesses and Bearing Capacity.

The bearing capacity of a dynamic pressure radial bearing with spiral grooves at various spiral angles has been simulated and analyzed. As illustrated in Fig 6, the bearing capacity initially increases and then decreases as the spiral angle increases. This phenomenon occurs because a larger spiral angle diminishes the pumping effect, leading to a reduction in bearing capacity. The optimal spiral angle for achieving maximum bearing capacity is between 50° and 60°.

(2) The Effect of Different Film Thickness on the Bearing Capacity of the Gas Film

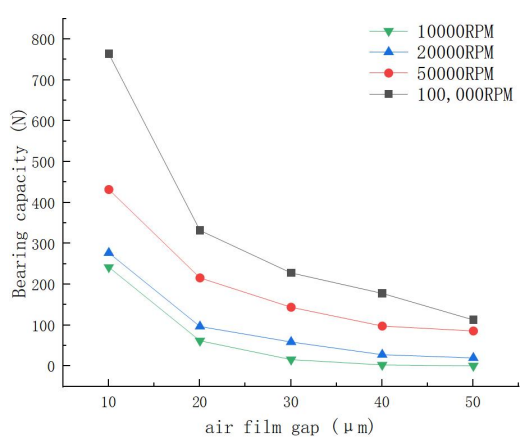


Fig 7. The Relationship Between Different Air Film Thicknesses and Bearing Capacity.

The effect of film thickness on bearing capacity demonstrates that an increase in film thickness leads to a decrease in bearing capacity. A simulation analysis of spiral groove hydrodynamic radial bearings with varying gas film thicknesses reveals the relationship between bearing capacity and rotational speed, as illustrated in Fig 7.

(3) The Effect of Different Eccentricities on the Bearing Capacity of the Gas Film

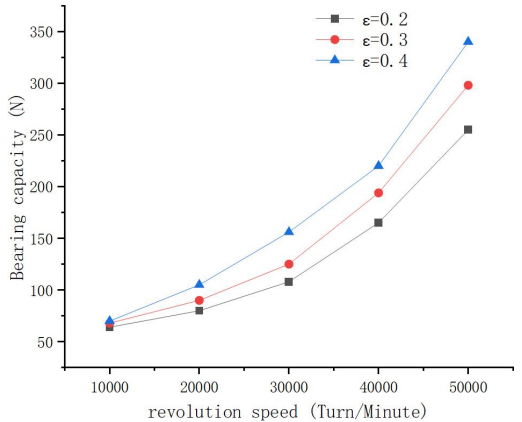
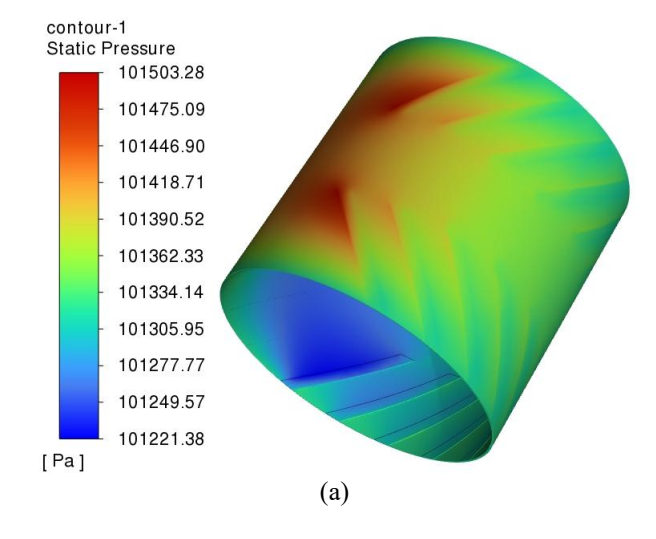


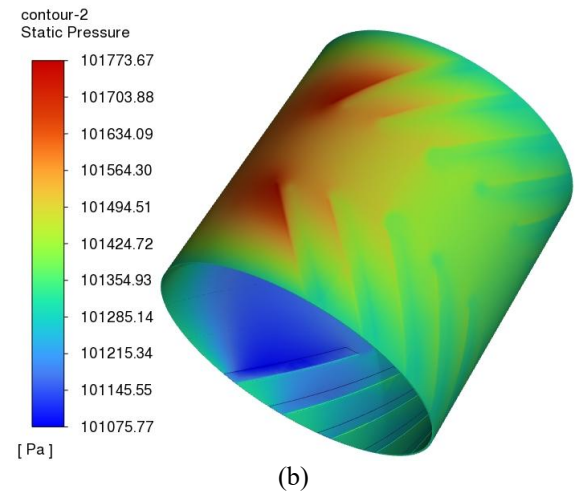
Fig 8. Relationship Between Different Speeds and Load Capacity.

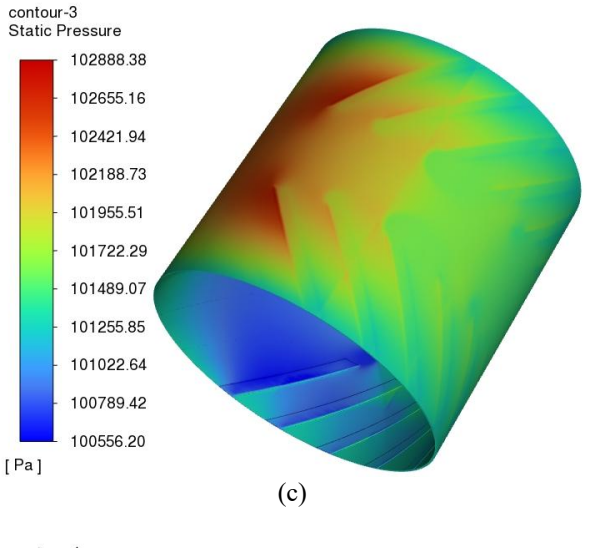
The rotational speed reveals a trend of increased load capacity as the speed increases from 10,000 to 50,000 revolutions per minute. A simulation analysis of the dynamic pressure radial bearing, which incorporates spiral grooves at different speeds, illustrates the relationship between load capacity and spiral angle, as shown in Fig 8.

(4) Different speed simulation cloud

Fig 9 presents a three-dimensional gas film pressure contour map of the spiral groove dynamic pressure[15] radial bearing[16], generated using Fluent post-processing, with an eccentricity ratio of 0.4.







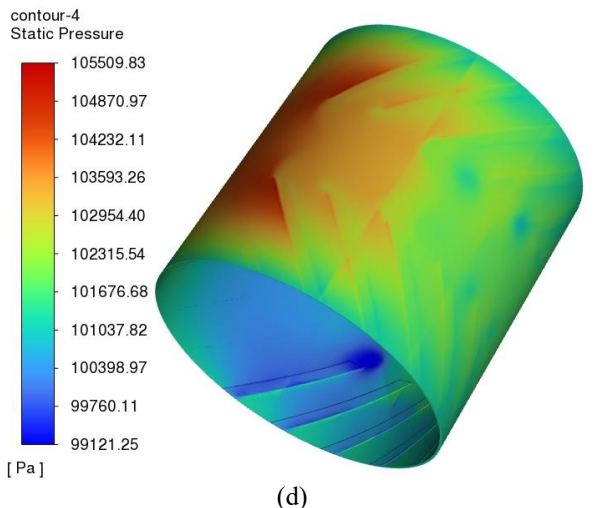


Fig 9. Comparison of Simulation Results.

Pressure contour maps at rotational speeds of 10,000, 20,000, 50,000, and 100,000 rpm are shown in Figures (a), (b), (c) and (d), respectively. The red high-pressure area demonstrates the most significant dynamic pressure effect and the highest pressure within the narrow gas film gap. In contrast, the blue low-pressure area exhibits a minimal dynamic pressure effect and lower pressure in the wider gas film gap. The presence of eccentricity creates a pressure disparity between the high-pressure and low-pressure zones. As speed increases, this pressure difference becomes more pronounced, resulting in an enhancement of bearing capacity.

V. ALGORITHM

A. Plackett-Burman Optimization Process

To determine the optimal [17] parameters for achieving sufficient bearing capacity, several influencing factors must be considered. This research employed the Plackett-Burman test[18] using Design-Expert to improve the test results.

Fig 10 illustrates that among the various structural parameters influencing the load capacity of the gas bearing, air film gap (C) plays the most significant role, with its Pareto contribution far exceeding those of the other factors. Following it are the spiral angle (A) and eccentricity (B), while flute width (D) and flute depth (E) have smaller yet still important effects.

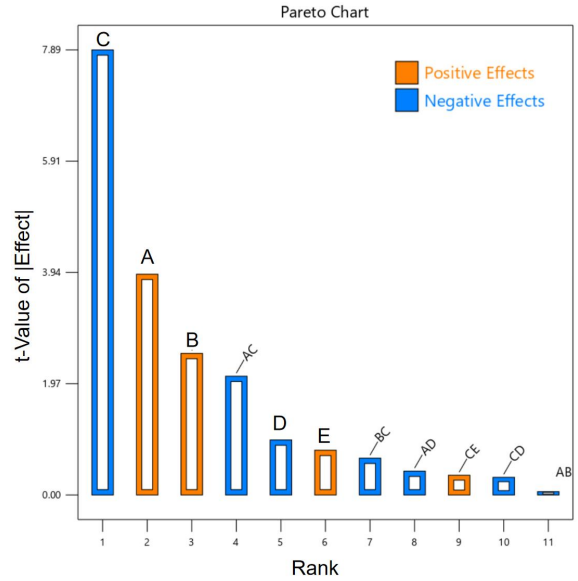


Fig 10. Diagram Parameter Effects

In the figure, orange bars indicate positive impacts, meaning that as the parameter value increases, the load capacity consistently rises; blue bars indicate negative impacts, where increasing the parameter value results in a decrease in load capacity. Notably, the load capacity is highly sensitive to changes in film thickness, with even minor variations causing substantial shifts in load capacity. This sensitivity has been thoroughly confirmed through experiments employing a BP neural network. Therefore, detailed optimization within the multi-parameter coupled space and careful coordination of the relationships among helix angle, eccentricity, groove width, groove depth, and film thickness are crucial for achieving overall optimization of the load capacity.

B. Optimal Latin Hypercube Design

The optimal Latin hypercube design aims to enhance the uniformity and representativeness of sample point distribution by employing an optimization [19] algorithm. This approach seeks to achieve high efficiency and accuracy in test results, minimize experimental errors and costs, and effectively manage complex multi-parameter systems. In this research, five parameters—gas film gap, eccentricity, spiral angle, groove width, and groove depth—were identified using optimal Latin hypercube design, resulting in 30 sets of random parameter combinations, as illustrated in Fig 11. Table II presents the ranges from which these parameters were selected, with each geometric variable constrained by minimum and maximum values that together define the permissible design space analyzed in this study.

TABLE II
PARAMETER SELECTION RANGE

Geometric parameters	Lower bound	Upper bound
air film gap (μm)	10	50
spiral angle (°)	20	60
eccentricity	0.3	0.5
flute width (mm)	1.6	2.9
flute depth (μm)	13	33

 ${\bf Five-factor Latin hypercube sampling (Color: Flute\ depth, Size: Flute\ width)}$

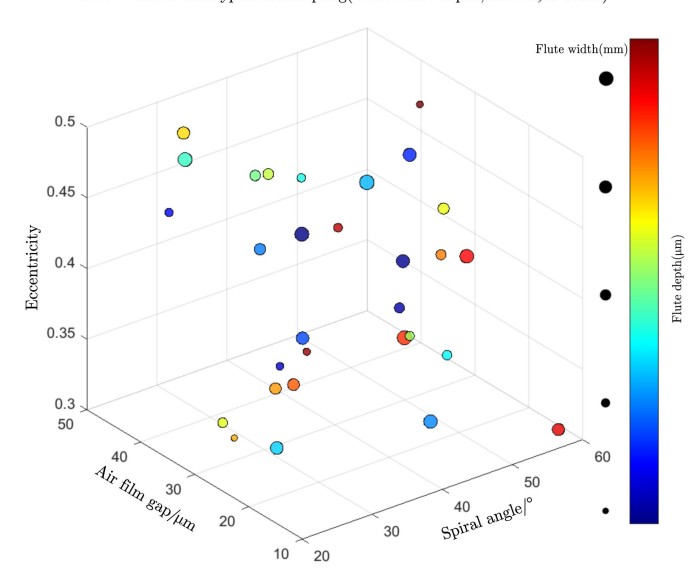


Fig 11. Optimal Latin Hypercube Selection Parameter Space Distribution Map.

C. Enhanced Particle Swarm Algorithm for Neural Network Optimization

The training of neural networks centers on two primary objectives: accelerating convergence and improving model performance. The Improved Particle Swarm Optimization (IPSO) algorithm can significantly expedite the training of Backpropagation (BP) neural networks, enabling them to achieve convergence more quickly and attain enhanced performance. Unlike traditional BP neural networks, IPSO exhibits robust global search capabilities that assist the network in avoiding local optima, resulting in superior overall solutions and a notable enhancement in network performance.

The IPSO-BP consists of three layers: an input layer, a hidden layer, and an output layer, as illustrated in Fig 12. This study focuses on optimizing the bearing capacity of the spiral groove hydrodynamic radial bearing under specified design conditions. The optimization variables include gas film clearance h, spiral angle β , eccentricity ε , groove width W, and groove depth M. The IPSO-BP neural network is utilized to model the relationship between these independent variables and the optimization objectives. The established mapping relationship is presented in equation (4):

$$(F) = P(h, \beta, \varepsilon, W, M) \tag{4}$$

In the equation (4), P represents the relationship established by the neural network between the optimization objectives and the independent variables h, β , ε , W, and M.

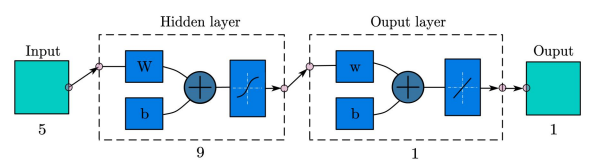


Fig 12. IPSO-BP Neural Network.

D. Comparison of Performance of Different Algorithms

An analysis of the prediction outcomes from the traditional backpropagation (BP) neural network, the improved particle swarm optimization BP (IPSO-BP) neural network, and the genetic algorithm-based BP (GABP) neural network reveals that the IPSO-BP neural network's predictions are more closely aligned with the actual values. This method exhibits a smaller prediction error compared to both the traditional BP and GABP methods, resulting in greater accuracy. The fitting graph comparing the predicted and actual values is illustrated in Fig 13, while the prediction error values are presented in Fig 14.

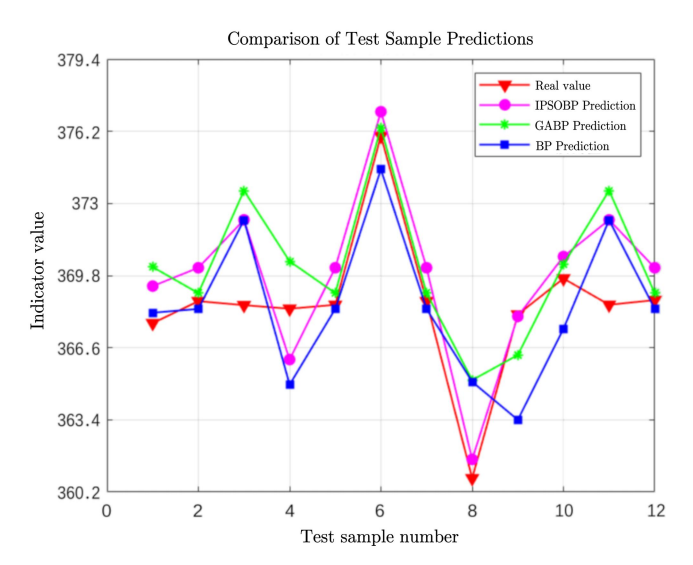


Fig 13. Fitting Diagram of Predicted Value and Real Value.

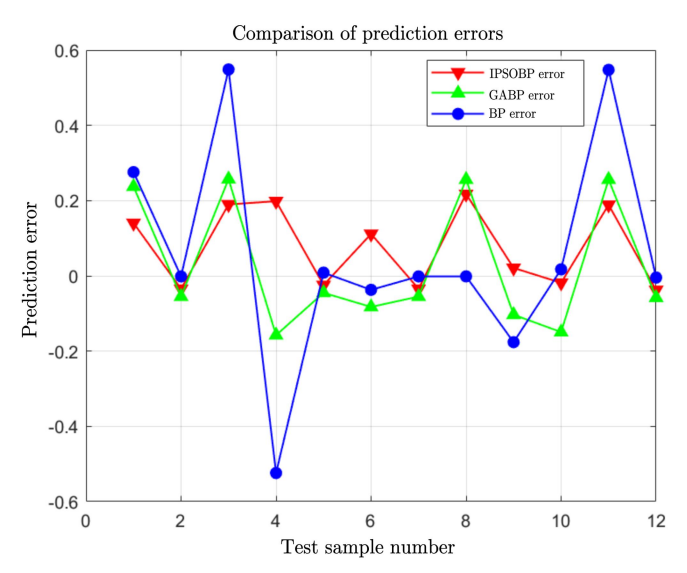


Fig 14. Prediction Error Value.

E. Genetic algorithm optimization

Utilizing a genetic algorithm inspired by Darwin's theory of biological evolution, this approach simulates the process of biological evolution to harness the global optimization capabilities of the genetic algorithm in identifying the geometric parameters that yield optimal performance for spiral groove bearings. The population size is set at 50, with a maximum of 100 iterations, and the genetic algorithm is executed 10 times to reduce randomness and achieve a more consistent and reliable optimized structure. The data comparing the results before and after optimization is presented in Table III.

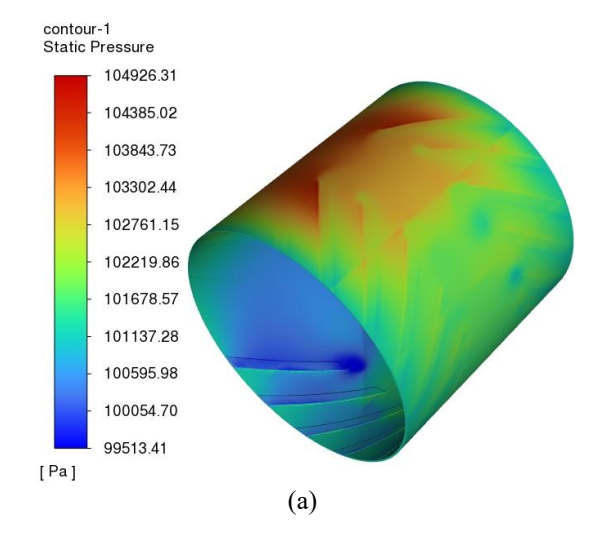
TABLE III
DATA COMPARISON BEFORE AND AFTER OPTIMIZATION

Prior to and following optimization	Before optimization	After optimization
Air film gap h/(μm)	15	10.3
Spiral angle $\beta/(^{\circ})$	45	51.6
Eccentricity	0.3	0.4
Flute width /(mm)	2.5	2.25
Flute depth /(µm)	13	15.2
Bearing capacity /N	363.3	377.4

The refined structural parameters—gas film thickness of $10.3~\mu m$, eccentricity of 0.4, spiral angle of 51.6° , flute width of 2.25~mm, and flute depth of $15.2~\mu m$ —were utilized in a Fluent simulation, resulting in a bearing capacity of 377.4~N. This represents a significant improvement compared to the original parameters. The optimized bearing capacity increased from 363.3~N to 377.4~N, reflecting a gain of 3.9%, or 14.1~N. This outcome demonstrates the effectiveness of the optimization method in enhancing the bearing capacity of the hydrodynamic spiral groove bearing.

F. Comparison before and after optimization

The optimization algorithm is employed to improve five parameters: gas film clearance, eccentricity, spiral angle, groove width, and groove depth. This enhancement results in the pressure cloud diagram of the bearing at 100,000 revolutions, as illustrated in Fig 15.



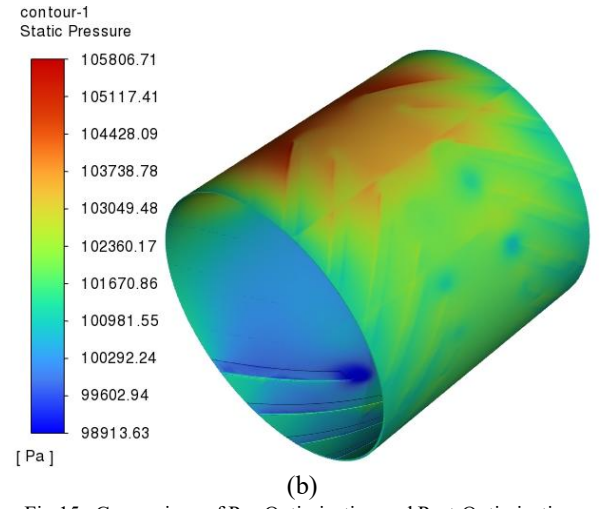
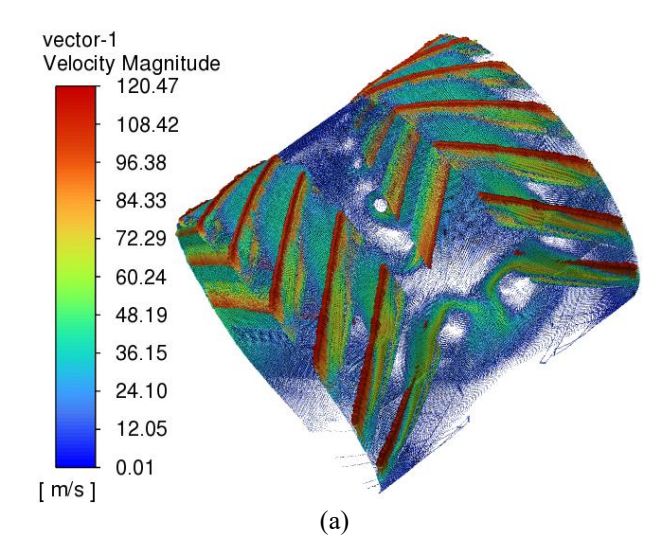


Fig 15. Comparison of Pre-Optimization and Post-Optimization.

Fig (a) shows the simulation cloud map before optimization, while Fig (b) displays the simulation cloud map after optimization. Prior to optimization, the pressure distribution in the spiral groove gas film is highly concentrated. After optimization, the pressure distribution becomes more uniform, which enhances the stability of the bearing and increases the pressure difference between the high and low-pressure zones, significantly boosting the bearing capacity. By refining the parameters, more effective design specifications are achieved, providing valuable insights for theoretical production.



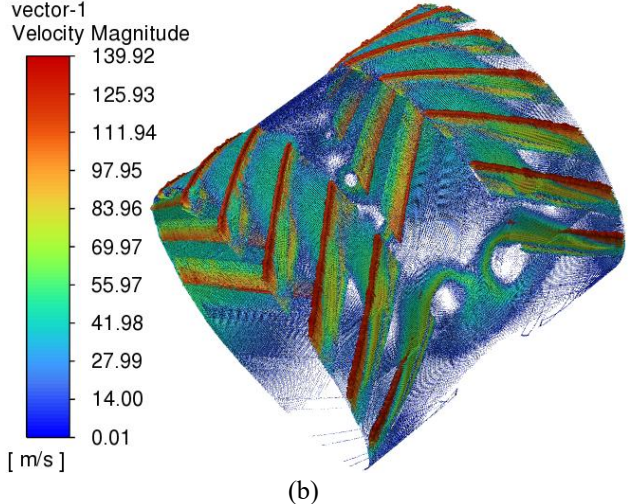


Fig 16. Flow Regions Before and After Optimization

Fig 16 shows the flow field regions before and after optimization. Fig (a) illustrates the flow field area before optimization, where the velocity gradually decreases from 120.47 m/s at the center to 0.01 m/s near the edges, exhibiting a smooth gradient and a limited high-speed zone. In contrast, Fig (b) shows the same area after optimization, with an increased maximum velocity of 139.92 m/s and a steeper gradient. The optimized flow field exhibits a higher peak velocity[20] and a steeper velocity gradient, indicating an improved throttling effect and increased dynamic pressure, which significantly enhances load-bearing capacity. The minimum velocity remains at 0.01 m/s with no backflow leakage, thereby minimizing energy loss. Adjustments to the air film gap and spiral groove parameters have successfully achieved a balance between high stiffness and stability,

meeting the design objectives.

G. Analysis of Low-Speed and High-Speed Segments Before and After Optimization

During the start-stop and low-speed phases of the spiral groove dynamic pressure radial air bearing, the gas dynamic pressure effect has not fully developed, resulting in insufficient gas film formation and a decrease in gas transmission efficiency. Fig 17 illustrates the gas film pressure distribution under low-speed start-stop conditions, both before and after optimization.

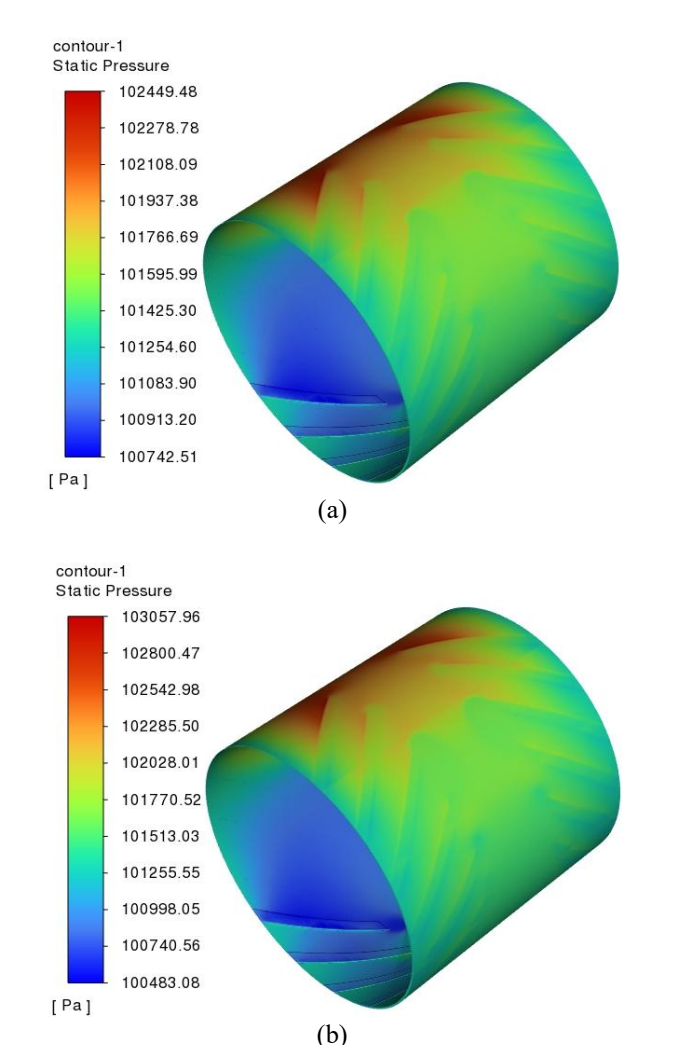


Fig 17. Comparison Chart of 50,000RPM: Before and After Optimization.

Fig (a) shows the contour map before optimization during low-speed startup, while Fig (b) displays the contour map after optimization during the same phase. During the low-speed start-stop phase, the distribution of the low-pressure zone within the pressure cloud, achieved through optimized parameters, becomes more uniform. This uniformity facilitates gas pumping, enabling the rapid formation of the gas film and minimizing its instability in the low-speed region. At a speed of 50,000 RPM, the bearing capacity of the spiral groove bearing is 310.7 N, which increases to 342.7 N after optimization, representing a 10.3% improvement. This indicates a significant enhancement in the bearing capacity of the optimized design during the low-speed phase.

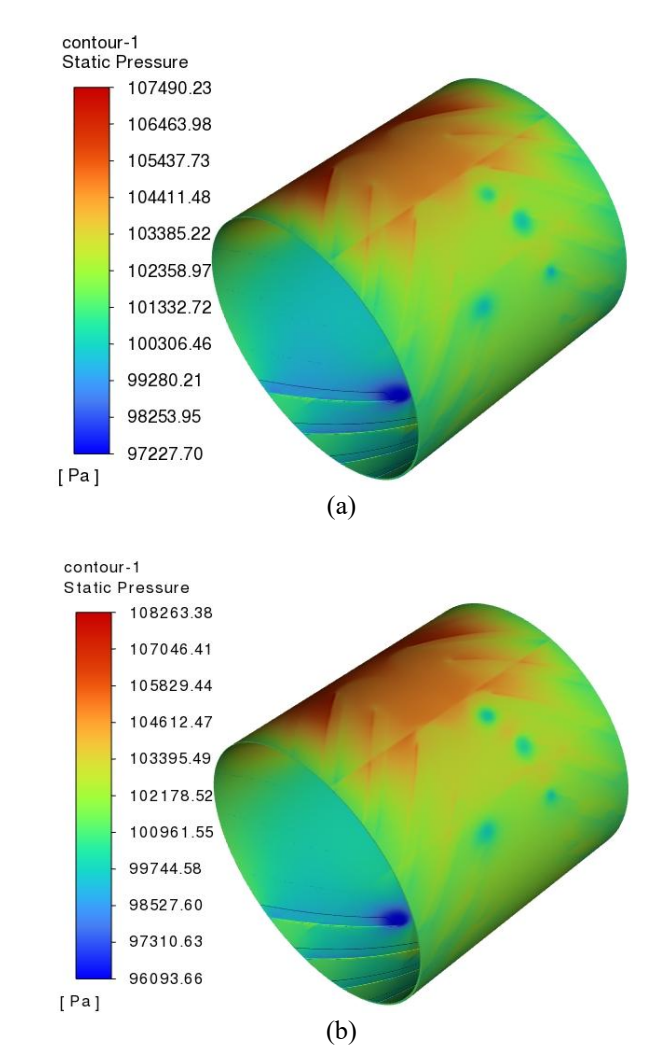


Fig 18. Comparison Chart of 150,000RPM: Before and After Optimization.

Fig (a) shows the cloud map before optimization during high-speed stable operation, while Fig (b) displays the cloud map after optimization during low-speed startup. At high speeds, the gas film demonstrates remarkable stability, leading to a substantial pressure differential between the high-pressure and low-pressure regions, which improves bearing capacity. Fig 18 presents the pressure cloud diagram of the spiral groove bearing operating at 150,000 RPM. The bearing capacity before optimization was 417.7 N, while after optimization, it increased to 432.9 N, indicating a rise of 3.6%.

The optimization approach significantly enhances the load-bearing performance of the gas film bearing at low speeds by improving the uniformity of the gas film thickness and increasing the pumping effect, resulting in more than a 10% increase in load capacity. This improvement effectively strengthens the equipment's ability to carry loads and maintain stable operation during startup and low-speed phases. During high-speed operation, since the initial hydrodynamic pressure already plays a dominant role, the optimization strategy provides only a modest additional load capacity increase of 3.6%. Nevertheless, its primary benefit at high speeds is the effective suppression of system instability, significantly reducing the likelihood of gas film oscillations and instability, thereby enhancing operational reliability and safety under these conditions.

VI. CONCLUSION

This research presents a Backpropagation (BP) neural network optimization technique that integrates an enhanced particle swarm optimization algorithm into the training of artificial neural networks. By establishing an approximate relationship between the bearing capacity and the bearing parameters of the aerodynamic pressure gas bearing identified by the algorithm, and utilizing genetic algorithm optimization, the bearing capacity of the spiral groove dynamic pressure radial bearing is significantly improved. Aerodynamic analysis and validation lead to the following conclusions:

- 1) The particle swarm optimization algorithm is integrated into the training of artificial neural networks, improving the accuracy of the relationship between the air bearing's load capacity and its bearing parameters.
- 2) The Improved Particle Swarm Optimization (IPSO) neural network has been enhanced to establish an approximate relationship between bearing capacity and the parameters of gas dynamic pressure air bearings. The bearing parameters optimized through the genetic algorithm exhibit significant adaptability across a range of speeds.

REFERENCES

- Y. Dong, Y. Niu, Y. Wang, et al., "Research on aerodynamic performance analysis of micro radial spiral-grooved air bearing," Engineering Research Express, vol. 5, no. 1, p. 015001, 2023.
 Z. Le, X. Qi, W. Bo, et al., "Study on the capacity performance of
- [2] Z. Le, X. Qi, W. Bo, et al., "Study on the capacity performance of journal bearings with different spiral groove structures by CFD method," IOP Conference Series: Materials Science and Engineering, vol. 999, no. 1, p. 012015, 2020.
- [3] J. Shi, B. Zhao, J. He, et al., "The optimization design for the journal-thrust couple bearing surface texture based on particle swarm algorithm," Tribology International, vol. 198, pp. 109874-109874, 2024.
- [4] B. Wang, Dynamic Pressure Gas Bearing Dynamics Calculation and Analysis [D]. Tianjin University, 2019.
- [5] Z. Dong, Y. Yu, Y. Dong, et al., "Application of BP Neural Network in the Optimization of Centrifugal Compressor Impellers," Automotive Practical Technology, vol. 50, no. 02, pp. 56-62, 2025.
- [6] L. Zhang, Analysis of the Fluid Dynamic Characteristics of Sliding Bearings with Spiral Groove Shapes [D]. Nanjing Forestry University, 2019.
- [7] S. Li, J. Sun, W. Cui, "Research on the Load-Bearing Characteristics of Human-Shaped Groove Small Hole Throttle Static Pressure Gas Bearings," Lubrication and Sealing, vol. 45, no. 06, pp. 34-38+60, 2020.
- [8] T. Liu, Z. Dong, "Comparison of the Performance of Radial Static Pressure Air Bearings with Different Cavity Structures," Lubrication and Sealing, vol. 48, no. 05, pp. 103-109, 2023.
- [9] H. Wang, Z. Dong, "Research on the Load-Bearing Characteristics of Spiral Groove Dynamic Pressure Radial Gas Bearings," Lubrication and Sealing, vol. 47, no. 06, pp. 65-72, 2022.
- [10] H. Hu, Research on Key Technologies of Conical Foil Gas Dynamic Bearings [D]. Beijing University of Science and Technology, 2023.
- [11] X. Jie, "A New Method for Analyzing Gas Spiral Groove Radial Bearings," Journal of Beijing University of Aeronautics and Astronautics, no. 03, pp. 112-117, 1990.
- [12] X. Pang, K. Niu, S. Wei, "Study on the dynamic pressure characteristics of radial bearings with a general film thickness equation using CFD methods," China Mechanical Engineering, vol. 23, no. 21, pp. 2521-2524, 2012.
- [13] H. Wang, Research on the Aerodynamic Characteristics of Radial Bearings with Spiral Grooves in Fuel Cell Air Compressors [D]. Taiyuan University of Science and Technology, 2022.
- [14] H. Xun, L. Shengye, L. Jinhao, "Modelling approach of hybrid air herringbone grooved journal bearing considering the angular misalignment and centrifugal expansion," Tribology International, vol. 189, 2023.
- [15] V. N. Thang, "Analytical study of the velocity of the lubricating fluid in the hydrodynamic journal bearing with the effect of centrifugal force

- for short bearing type," EUREKA: Physics and Engineering, no. 4, pp. 93-100, 2022.
- [16] Z. Lu, M. Wei, B. Liu, et al., "Analysis of Gas Film Pressure in Conical Spiral Groove Gas Dynamic Bearings," Journal of Xi'an University of Technology, no. 03, pp. 224-228 + 234, 2008.
- [17] Y. Wang, X. Liu, Y. Zhou, et al., "Parameter Optimization and Performance Analysis of Fuel Cell Centrifugal Compressor Impeller Configuration," Journal of Xi'an Jiaotong University, vol. 56, no. 06, pp. 164-174, 2022.
- [18] P. Y. An, J. X. Wang, L. Xiao, et al., "Optimization of Fat Substitute Preparation Using Plackett-Burman Experimental Design Combined with Box-Behnken Response Surface Method," Food Science, vol. 41, no. 10, pp. 255-264, 2020.
- [19] C. Zhikai, H. Haiyang, C. Qinlong, et al., "Novel multidisciplinary design and multi-objective optimization of centrifugal compressor used for hydrogen fuel cells," International Journal of Hydrogen Energy, vol. 48, no. 33, pp. 12444-12460, 2023.
- [20] Y. F. Huang, "Research on the generation method of rotating uniform airflow field based on reverse wind tunnel principle," M.S. thesis, Chongqing University, 2022.